A01-3

Model Construction for Computational Anatomy: Progress Overview FY2009-FY2013

Hiroshi Fujita [#1], Takeshi Hara [#1], Xiangrong Zhou [#1], Chisako Muramatsu [#1], Naoki Kamiya [#2], Min Zhang [#1], Daisuke Fukuoka [#3], Yuji Hatanaka [#4], Tomoko Matsubara [#5], Atsushi Teramoto [#6], Yoshikazu Uchiyama [#7], Huayue Chen [#8], and Hiroaki Hoshi [#9]

[#1] *Department of Intelligent Image Information, Division of Regeneration and Advanced Medical Sciences,*
Graduate School of Medicine, Gifu University, Gifu-shi, 501-1194 Japan
[1] `{fujita,hara,zxr,chisa,min}@fjt.info.gifu-u.ac.jp`

[#2] *Department of Information and Computer Engineering, Toyota National College of Technology,*
2-1 Eiseicho, Toyota, Aichi, 471-8525 Japan
[2] `n-kamiya@toyota-ct.ac.jp`

[#3] *Department of Technology Education, Faculty of Education, Gifu University, Gifu-shi, 501-1193 Japan*
[3] `dfukuoka@gifu-u.ac.jp`

[#4] *Department of Electronic Systems Engineering, School of Engineering, the University of Shiga Prefecture,*
Hassaka-cho 2500, Hikone-shi, Shiga 522-8533, Japan
[4] `hatanaka.y@usp.ac.jp`

[#5] *Department of Information and Media Studies, Faculty of Information and Media Studies, Nagoya Bunri University,*
Maeda-365 Inazawacho, Inazawa-shi, Aichi 492-8520 Japan
[5] `matsubara.tomoko@nagoya-bunri.ac.jp`

[#6]*Faculty of Radiological Technology, School of Health Sciences, Fujita Health University,*
Toyoake-shi, 470-1192 Japan
[6] `teramoto@fujita-hu.ac.jp`

[#7]*Department of Medical Physics, Faculty of Life Science, Kumamoto University,*
4-24-1 Kuhonji, Kumamoto-shi, 862-0976, Japan
[7] `y_uchi@kumamoto-u.ac.jp`

[#8] *Department of Anatomy, Graduate School of Medicine, Gifu University, Gifu-shi, 501-1194 Japan*
[8] `huayue@gifu-u.ac.jp`

[#9]*Department of Radiology, Graduate School of Medicine, Gifu University, Gifu-shi, 501-1194 Japan*
[9] `hoshi@gifu-u.ac.jp`

Abstract— **This paper describes the purpose and summary of our progress in the research work, which is a part of research project "Computational anatomy for computer-aided diagnosis and therapy: Frontiers of medical image sciences" funded by Grant-in-Aid for Scientific Research on Innovative Areas, MEXT, Japan. The main purpose of our research in this project is to be engaged in model construction of computational anatomy and CAD applications for automatically recognizing the anatomical structures of organ/tissue as well as lesions and analyzing the functions of different organs in whole body region based on different image modalities such as X-ray CT images, MR images, FDG-PET images, eye fundus photographs, dental panoramic radiographs and ultrasound images. In the whole term (five years) of this project, six progresses in anatomical model construction and more than nine progresses in CAD developments have been achieved. These progresses show the efficiency and potential usefulness of the proposed research works by the promising results.**

I. INTRODUCTION

Modern imaging devices represented by CT, MRI, and PET have been widely used in clinical medicine. The high performance of such scanners can provide detailed information of the whole body region, not only showing real anatomical structures of the patient in 3D, but also being able to visualize the functions of the inner organs within a short time.

Therefore, these medical images have been regarded as an important reference for screening, precise diagnosis, and surgery purposes in clinical medicine.

Medical images typically include a lot of diagnostic information that need to be interpreted by the doctors. For example, a torso CT scan generally generates 800-1200 2D axial slices and causes a lot of interpretation burdens for radiologists. Computer-aided diagnosis (CAD) can help to reduce such burden and assist image interpretation [1]. In order to realize a future-CAD that aims to do multi-disease detection on multi-organ regions from multi-modality images, automatic recognition of the detailed anatomical structures of organ/tissue as well as lesions and constructing the model of the normal human body are required [2]; however, it is a challenging issue. As one of the solutions, modelling the human anatomy and function for normal human body and abnormal lesions based on a large number of medical images is expected as one of the key techniques [3-5].

II. ACHIEVEMENTS

Our research activities have been focused on the novel developments in two research topics; one is the model construction and the other is CAD applications. These activities were followed on our research plan. The overview and relationship of these subjects are shown in Figure 1. We pick up the progress and summary in six research subjects as examples and describe each progress in the following section.

A. An universal organ segmentation approach based on machine-learning and similar image retrieval [6-14]

Purpose: The aim of this research subject was to model the process of organ segmentations and develop a universal scheme that can be used to segment the different solid organ regions automatically on CT images in the same way. We simplified the organ segmentation process by finding its location in CT images, retrieving and using the similar organ patterns in a database as the reference, and separating the organ and background by an optimization of a cost function. The proposed approach was a target-free segmentation method
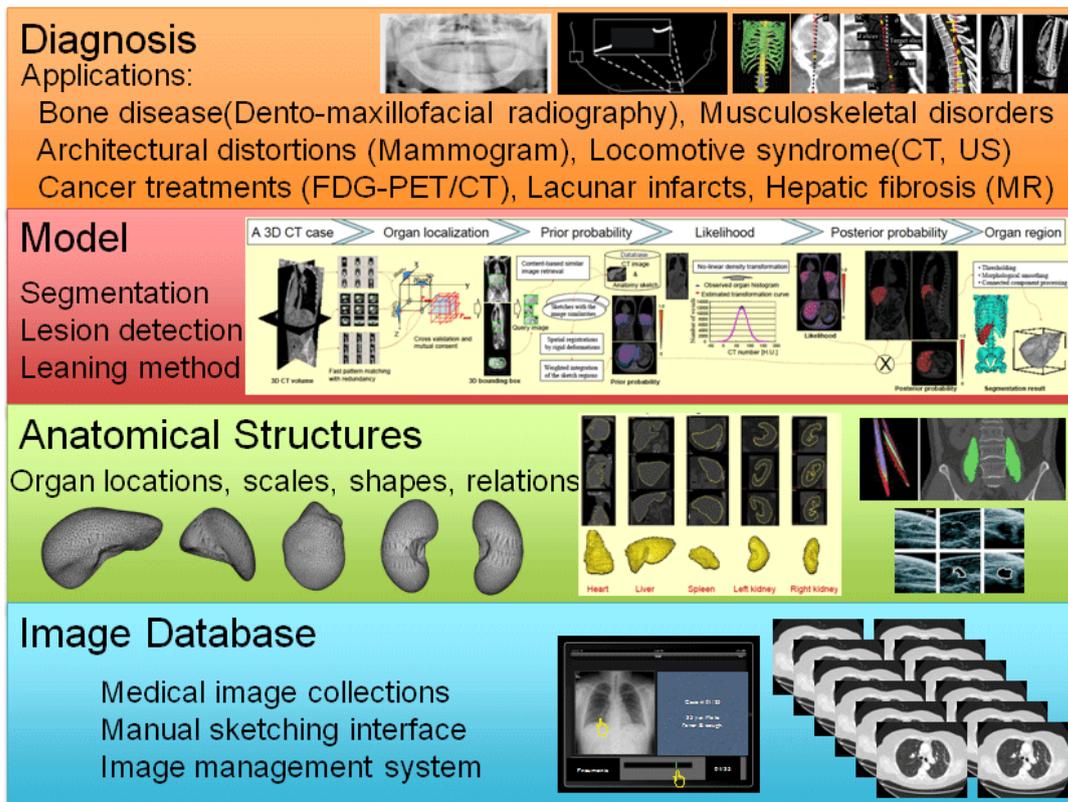
Fig. 1 Overview of our achievements
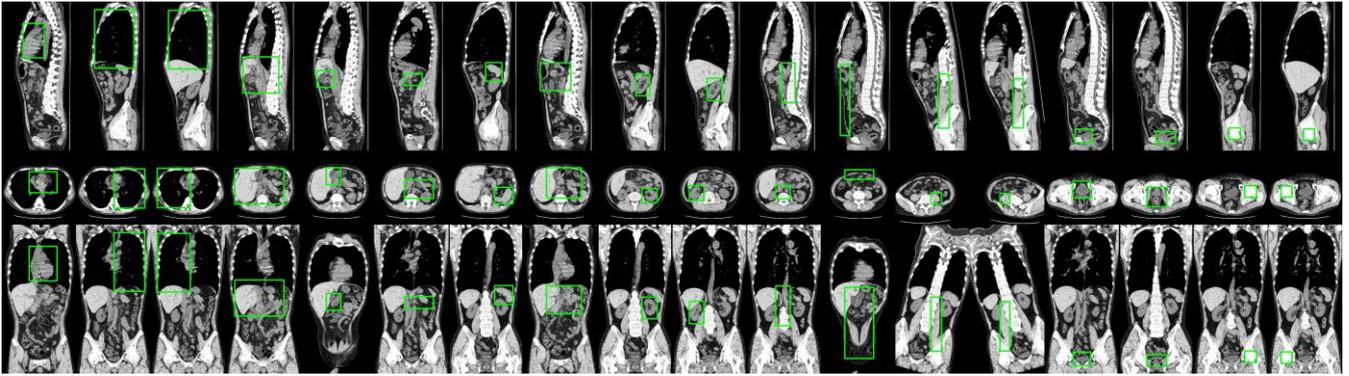
Fig. 2 An example of the localization results for 18 kinds of major organs and tissues in a 3D CT scan. Three slices that pass through the detected center position of the target organ are shown. The rectangle indicates the detected organ location (bounding rectangle of the heart, left-lung, right-lung, liver, gallbladder, pancreas, spleen, stomach, left-kidney, right-kidney, IVC & ventral aorta, abdominal rectus muscles, left-psoas-major-muscle, right-psoas-major-muscle, bladder, uterus & rectum, left-femur-head, and right-femur-head, from the left to right sides).

and fully based on machine-learning and data-driven methods. The advantage was that this approach uses more image data instead of complex algorithms to enhance the robustness and accuracy of the segmentation process [6-10].

Methodology overview: We modelled the different organ segmentation processes as two standard modules: "object detection" and "organ / background separation", and included three processing steps: (1) automated target organ localization based on machine-learning [7,9], (2) content-based image retrieval and patient-specific atlas construction [6], and (3) foreground / background separation by using iterated Graph-cuts based on atlas [10]. The features in methodology were that, for step 1, we proposed a 2D-detection and 3D-voting structure to realize a robust organ localization task by using a small number of training images; for step 2, we used a phase-correlation registration based on the fast Fourier transform (FFT) to accomplish a fast calculation of similarity measure of organ appearances in different CT images; and for step 3, we combined probabilistic atlas with the graph-cuts method to obtain a better result for organ segmentation on CT images.

Results: Two databases (DBs) that included more than 1000 cases of 3D volumetric CT cases were used for performance evaluations. These CT cases were collected at Gifu University hospital and Tokushima University hospital by three kinds of multi-slice CT scanners (LightSpeed Ultra16 of GE

Healthcare, Aquilion of Toshiba, and Brilliance 64 of Philips Medical Systems). Eighteen kinds of organ and tissue regions of heart, left- and right-lungs, liver, gallbladder, pancreas, spleen, stomach, left- and right-kidneys, IVC and ventral aorta, abdominal rectus muscles, left- and right-psoas-major-muscles, bladder, uterus and rectum, left- and right-femur-heads were selected as the targets for organ localizations and nine kinds of solid regions (liver, heart, spleen, gallbladder, bladder, left/right kidney, left/right psoas major muscle) were selected for evaluating the performance of the segmentation process.

We confirmed that the locations of 18 kinds of organs can detected correctly in more than 90% CT cases in two DBs. One example is shown in Fig.2. Nine kinds of massive organ regions can be segmented by our proposed scheme as shown in Fig.3. The ground truth of those organs in about 100 CT cases were manually extracted, and we found that the average coincidence ratios (JSC values) of all kinds of organs between automated segmentation results and ground truth were distributed from 0.79 to 0.91. These results indicate that our proposed scheme was very robust for different organ segmentations in both normal and abnormal CT cases. The segmentation results of massive organs were comparable to the manual inputs of the human operators [10].

Conclusion: We proposed a universal scheme for the segmentation of different organ regions automatically in 3D CT cases. This scheme was
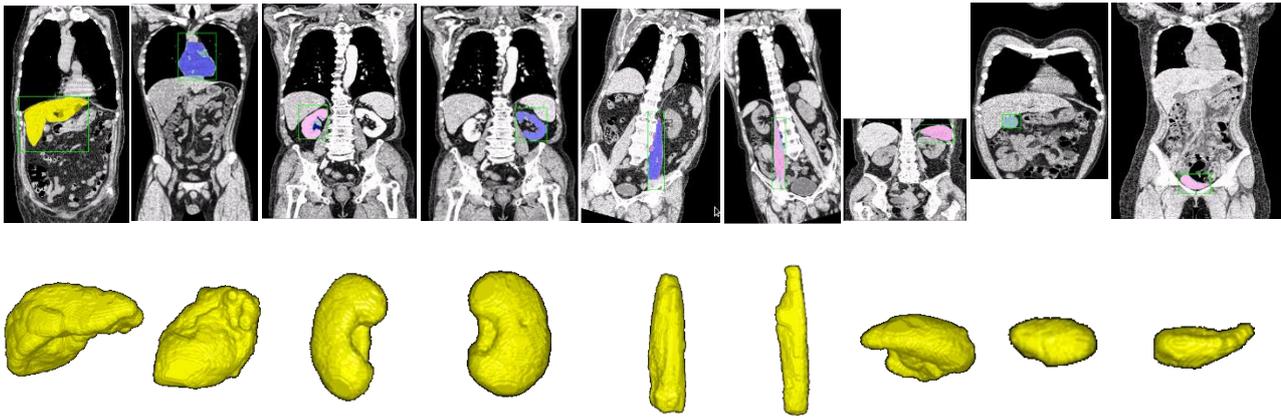
Fig. 3. An example of the segmentation results for 9 kinds of major organs and tissues in 3D CT scans. One coronal slice that passes through the detected center position of the target organ is shown. The segmented organ regions of liver, heart, right-kidney, left -kidney, left-psoas-major-muscle, right-psoas-major-muscle, spleen, gallbladder, and bladder are shown from left to right. The 3D contour of each segmented organ is visualized by using surface rendering and shown under the image.

applied to localize 18 kinds of targets and segment 9 kinds of solid organs form a large number (>1000) of CT images. The experimental results showed the efficiency and usefulness of proposed scheme for understanding and computing the human anatomy based on medical images.

B. A model-based approach to recognize deep and surface muscle region in CT images [15-18]

Purpose: In the super-aging society, for rehabilitation and extension of healthy life expectancy, accurate measurement of skeletal muscle volume is required. Our purpose is to develop a modelling technique of statistical shape model that takes into account the individual differences of skeletal muscle volume. Then, we develop site-specific automatic recognition techniques of the skeletal muscle using the generated shape model. We target two regions of the deep muscle and surface muscle. First, in the deep muscle, we target psoas major muscle region. Since psoas major muscle is located in the deep region, it is less sensitive to individual differences in body type. In the surface muscle, we target rectus abdominis muscle, latero abdominal muscle and trapezius muscle. The surface muscles are susceptible to individual differences in body size.

Methodology overview: Generally, shape model based method is effective when recognition target has a characteristic shape. Figure 4 shows the flow of the skeletal muscle recognition based on the shape models. First, the shape model is generated from training data. Then, anatomical feature points (landmarks: LMs) and virtual muscle fibers (centrelines) are automatically recognized on the test data. Finally, segmentation is achieved by fitting the shape model to the LMs and centrelines.

In the deep muscle, for example, the psoas major muscle has the spindle-shape. Shape model is generated from the manually segmented regions obtained for training data. The muscle contour is represented by using a mathematical function. In other words, an approximate curve (quadratic function) is set as a model for each centreline. In the recognition process, the shape model functions are fitted to test data. Then we calculate the fitting parameters representing the individual differences, and achieve the recognition.

In the surface muscle, individual differences in body type affect the fitting process of the shape model. Therefore, in order to simplify the body structure, we proposed a new method with a virtually projected image that is to unfold virtually a 3-D human body to a 2-D plane. It has been integrated into an automated recognition for surface muscles including rectus abdominis muscle, latero abdominal muscle and trapezius muscle. Secondly, to take into account the body differences on the virtually unfolded image, we improved the generating method of virtually unfolded image by the removal of subcutaneous fat region which is widely different between patients. The new method for generating the virtually unfolded image was proposed to simplify the body difference and to increase robustness of the anatomical feature

recognition on the images. Finally the muscle region was recognized on the image using shape model, which was indicated by the area, including all muscle fiber lines.

Results: In the five years of this research project, we achieved a good recognition performance for two types of muscle, a deep muscle, i.e., psoas major muscle, and surface muscles, i.e., rectus abdominis muscle, latero abdominal muscle and trapezius. Figure 4 (lower part) below shows the recognition result of each muscle region. The recognition performance for each muscle is 72.3% in psoas major muscle (80 cases) [15], 84.3% in rectus abdominis muscle (10 cases) [16], 83.0% in latero abdominal muscles (10 cases) [17] and 91.6% in trapezius muscle (6 cases) [18]. In conclusion, for the muscle recognition of deep muscle regions with small body differences, the statistical shape model is effective to detect muscle region. For the muscle recognition of surface regions with large body differences, the virtually unfolded image is effective to simplify the body variations. It suggests the possibility of an application of this method to the other muscle recognitions.

C. FDG-PET: Temporal subtraction for cancer treatments [19-22]

Purpose: Diagnostic imaging on FDG-PET scans was often used to evaluate chemotherapy results of cancer patients. Radiologists compare the changes of lesions' activities between previous and current examinations for the evaluation. Recently, an influence of fat components in body on SUV measurements is a typical issue in diagnosis because patients tend to lose their weight during the treatment. A normalized SUV (Standardized Uptake Value) by lean body (SUL or SUVbw) mass is recommended in PERCIST (evolving
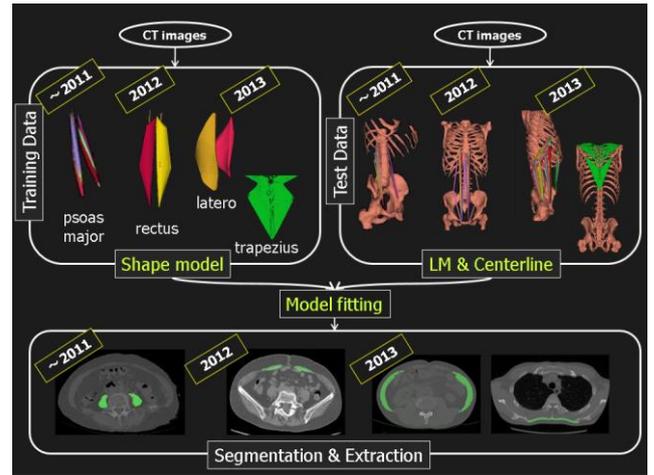
Fig.4 Recognition results of surface and deep muscle

considerations for PET Response Criteria in Solid Tumors). The normalized SUV was obtained by the original SUV, the patient body weight with fat, and height. To deal with the typical clinical issues, we aimed to construct a new normal model for torso FDG-PET by using SUL.

Methodology overview: Z-score mapping based on statistical image analysis was applied to the temporal subtraction technique. The subtraction images can be obtained based on the anatomical standardization results because all of the patients' scans were deformed into the standard body shape [19, 20].

An observer study was performed without and with CAD to evaluate the usefulness of the scheme by ROC (receiver operating characteristics) analysis. Readers were asked to set their confidence levels from absolutely no change to definitely change between two scan on a continuous scale [21].

To construct a new normal model based on SUL, each SUV in every locations of a patient was converted into SUL by using his/her body weight

Mean SD Male	Mean SD Male	Original Difference image Image
Mean SD Female	Mean SD Female	
(a) SUL normal model	(b) Differences between SUL and SUV normal model	(c) Example of abnormal spot in lung area
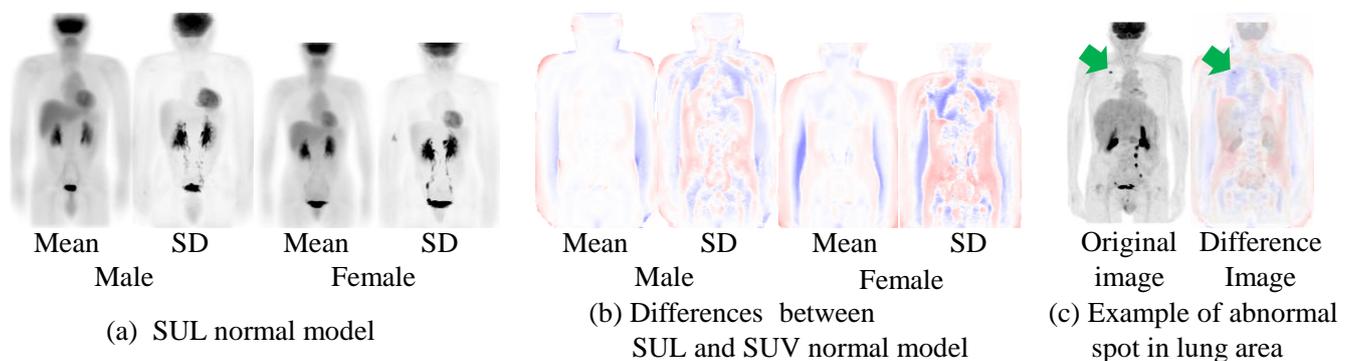
Fig.5 Effect of SUL normal model

and height. After the SUL distribution was obtained, the deformation process was applied to construct the standardized body shape. The same procedure to construct the normal SUV models was applied to the SUL model construction. The differences of voxel values between SUV and SUL normal models in each gender were obtained to compare the two models [22].

Results: The recognition performance for the 43 pairs was 96% sensitivity with 31.1 false-positive marks per scan. The average of area-under-the-ROC-curve (AUC) from four readers was increased from 0.85 without CAD to 0.90 with CAD (p=0.0389, DBM-MRMC).

The effect of SUV correction with lean body mass in lung and liver was confirmed on graph plots of BMI vs SUVs and SULs obtained from normal cases. Figure 5(a) shows the constructed normal model by using SUL distributions. Figure 5 (b) indicates the difference of voxel values between the SUV and SUL normal models. The values in lung regions in each gender were corrected in the SUL models. Abdominal regions were strongly affected by the fat components as shown on SD models in each gender. Figure 5(c) shows an example case with an abnormal spot in lung. The Z-score based on SUV model was 15.8, but the Z-score based on SUL model was 20.1. The abnormality of the spot was estimated appropriately in the SUL model.

We confirmed that the Z-score in torso FDG-PET scans by using not only SUV but also SUL was helpful in cancer diagnosis for screening, metastasis, and chemotherapy.

Conclusion: We have confirmed the fundamental usefulness of CAD system for torso FDG-PET scans to interpret temporal changes between two time series examinations such as chemotherapy or radiotherapy for cancer treatments. The Z-scores obtained by SUV and SUL normal models will be helpful indices as statistical reference values in interpreting a single examination.

D. Automated measurement of mandibular cortical width on dental panoramic radiographs by using mandibular contour model [23,24]

Purpose: Clinical studies have shown that the mandibular cortical width (MCW) measured on dental panoramic radiographs (DPRs) is significantly correlated with bone mineral density (BMD) in the hip, lumbar spine and femoral neck. Therefore, identifying asymptomatic patients with osteoporosis through dental examinations may bring a supplemental benefit to the patients. However, most DPRs are used only for diagnosing dental conditions by dentists in their routine clinical work, and the condition of the mandibular cortex is generally not paid attention. The purpose of this study is to develop an automated MCW measurement method for establishing a possible secondary screening path via dental examination.

Methodology overview: First, potential mandibular edges were detected by use of a mandibular mask and a modified Canny edge detector. The most similar mandibular contour model was selected from the training cases by the similarity score based on the distance transformation. The selected model was used as the initial model and fitted to the test case by an active contour method. The mental foramina positions of the fitted model, which were identified manually beforehand, were determined as the MCW measurement reference positions (Fig.6). Regions of interest were obtained by sampling the pixels from points along the mandibular contour around the reference positions to the perpendicular direction toward cavernous bone. Based on the line convergence analysis, the most suitable MCW measurement ranges and the border searching ranges were selected. Finally, the upper margins of the cortices were determined by the profile analysis.

Results: The correlation coefficient between the manual measurement by a dental radiologist and the proposed method was 0.91. The area under the receiver operating characteristic curve for distinction between osteoporotic cases and control cases was 0.963.

In the recent multi-clinic trials with cooperation
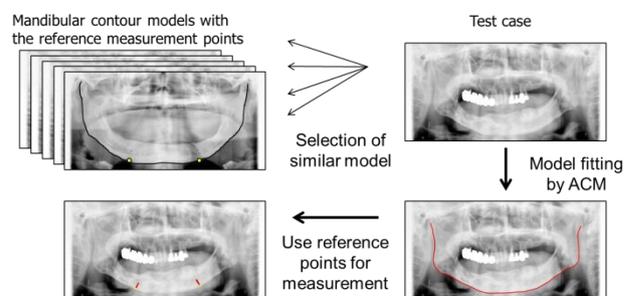
Fig.6 Model searching and fitting for mandibular contour extraction

to a cloud-based teleradiology service, 457 cases from 7 dental clinics were tested. Out of these, 21 cases were considered suspected osteoporosis. By use of our method, the sensitivity was 85.7% while the specificity was 81.0%. These suspected cases are likely unidentified in the routine dental examinations. The results indicate the potential utility of our CAD system for early diagnosis of osteoporosis.

E. Investigation of probabilistic models for differentiation of glaucoma from non-glaucoma eyes on retinal fundus images [25,27]

Background: Retinal fundus photography is frequently and widely used examination for diagnostic record, longitudinal comparison, and screening of eye diseases. Because it can visualize blood vessels non-invasively, it is sometimes imaged during health check-ups. In reading retinal fundus images, physicians must look for various signs of abnormalities. However, the number of qualified professional is limited, and reading many screening images is time consuming. Therefore, for reducing physicians' workloads and improving diagnostic efficiency, we have been investigating the computerized diagnosis and quantification systems for glaucoma, diabetic retinopathy, and hypertensive retinopathy.

For diagnosis of glaucomatous eyes, we have previously proposed the automated scheme for measuring cup-to-disc ratio (CDR) [25], which is one of the indices considered by ophthalmologists in the clinical practice. However, determination of cup border is sometimes difficult because of the absence of clear edges, especially for the non-glaucomatous eyes. To improve classification accuracy, we have investigated a new scheme that does not require segmentation of cup regions but uses probabilistic models of cup gradient information from training data. To our knowledge, no groups have investigated a model-based glaucomatous-disc differentiation scheme.

Methodology overview: For this study, stereo fundus images were used. First, the location of optic disc is automatically detected, and subsequently, the disc region is segmented by using an active contour model [26]. From a stereo pair, parallax was determined by searching the local corresponding points, and the depth image was

created [25]. Using training cases, we created models for glaucomatous and non-glaucomatous eyes by registering the disc border and averaging the depth gradient images. For registration, thin plate spline was applied to the sample points on the automatically segmented disc outlines. Figure 7 shows the examples of glaucomatous and non-glaucomatous disc images and their models [27]. In applying the models, similarity scores between the models and a test case were determined by multiplying the gradient image of the test case and the models. On the basis of the difference in the similarity scores, test cases were classified into glaucomatous or non-glaucomatous cases.

Results: The method was tested with 87 cases, including 40 glaucomatous eyes. By using CDR determined by our previous method, the sensitivity was 90.0% with the specificity of 83.0%. Using the proposed method, the specificity was improved to 97.9% at the same sensitivity level. Although automated measurement of CDR has some practical value because of its quantitativeness, the cup gradient information obtained by the proposed method can be useful in the diagnosis to supplement CDR. Further investigation is needed for improvement of both methods and combination of the schemes.
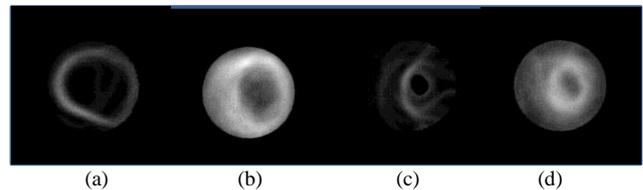
Fig.7 Examples of depth gradient images and their models. (a) glaucomatous eye, (b) glaucomatous model, (c) non-glaucomatous eye, and (d) non-glaucomatous model

F. CAD for detecting lacunar infarcts in MRI [28-31]

Purpose: The detection of lacunar infarcts is important because their presence indicates an increased risk of severe cerebral infarction. However, accurate identification is often hindered by the difficulty in distinguishing between lacunar infarcts and enlarged Virchow-Robin (VR) spaces. Therefore, we have developed CAD schemes for the detection of lacunar infarcts [28-31]. An observer study was also conducted to evaluate the performance of radiologists without and with use of the CAD scheme [28]. The mean area under the

ROC curves without and with computer output were 0.891 and 0.937, respectively. Therefore, we believe that the CAD scheme could improve the accuracy of radiologists' performance in the detection of lacunar infarcts. In the observer study, we realized that (1) some FPs due to enlarged VR spaces detected by the computer were difficult for radiologists to distinguish from lacunar infarcts. These FPs were the main sources to the detrimental effects of the CAD scheme. (2) The clear FPs had an impact on the reliability of the result of the computer. The purpose of this study is to improve our CAD scheme for the clinical application.

Methodology overview: (1) Lacunar infarcts were often detected in basal ganglion, optic thalamus, and cerebral deep white matter, whereas enlarged VR spaces were symmetrically detected in the lower third of basal ganglion. Therefore, we used anatomical location features for distinguishing between lacunar infarcts and enlarged VR spaces [29]. (2) We improved our CAD scheme for detection of lacunar infarcts by using template matching techniques in order to eliminate clear FPs such as a part of cerebral ventricle and a part of cerebral sulcus [30, 31].

Results: (1) The area under ROC curve for distinction between lacunar infarcts and enlarged VR spaces increased from 0.89 (without anatomical location features) to 0.93 (with anatomical location features). (2) By using AdaBoost template matching technique, 52.9% of FPs was eliminated while keeping the same sensitivity. The final sensitivity of the detection of lacunar infarcts was 96.8% with 0.33 FPs per slice.

III. CONCLUSIONS

Our progresses for anatomical model construction and applications based on multimodality medical images were described. We developed a universal solution for automatic organ and tissue segmentations and confirmed its usefulness and efficiency by applying to 18 kinds of organ localization and 9 kinds of organ regions based on more than 1000 CT cases. We also accomplished the muscle region segmentations by using shape models that had not been reported before. Those works are beneficial to the CAD developments by providing a possible way to recognize a number of anatomical structures quickly and automatically on CT images.

We also developed a whole body probabilistic model to show the metabolic activities of the normal organs and tissues based on FDG-PET images. This work showed the potential possibility of our consideration for detecting the lesions by comparing the patient image to a normal human body model. The proposition was made by our group for solving the problem of the multi-lesion detection in multi-organs.

Our model constructions and applications were also successfully applied to many CAD systems on retinal fundus images, dental panoramic radiographs, and MRI for supporting different lesion detection and classifications. As many other applications in author's group, different models were developed for pulmonary emphysema classifications on CT images [13, 14], lung nodule detection system based on CT and PET [32-34], distortion detection on mammograms [35], gastrocnemius muscle measurements on ultrasound images [36, 37], similarity-based CAD for breast mass diagnosis on mammograms [38, 39], and liver cirrhosis diagnosis [40-42]. The performance and usefulness of those models were confirmed by the promising results and published in many books and journals [44-50].

Our research group was collaborated with several research groups of the same research project. Especially, we have been working together with the Kido Lab. of Yamaguchi University and shared the image database and source codes of the programs each other for shape model constructions. The novel results of these research works have been presented in [11, 12, 43].

REFERENCES

[1] K.Doi: Computer-aided diagnosis in medical imaging: Historical review, current status and future potential, Computerized Medical Imaging and Graphics, Vol.31, 198–211, (2007).
[2] H.Kobatake: Future CAD in multi-dimensional medical images - Project on multi-organ, multi-disease CAD system, Computerized Medical Imaging and Graphics, Vol.31, pp.258–266, (2007).

[3] H.Fujita, T.Hara, X.Zhou, H.Chen, and H.Hoshi: Computational anatomy: Model construction and application for anatomical structures recognition in torso CT images, Proc. of the First International Symposium on the Project "Computational Anatomy", 58-61, (2010).

[4] H.Fujita, T.Hara, X.Zhou, T.Hayashi, N.Kamiya, H.Chen, and H.Hoshi: Model construction for computational anatomy: Progress overview FY2011, Proc. of the 3rd International Symposium on the Project "Computational Anatomy", 24-32, (2012).

[5] H.Fujita, T.Hara, X.Zhou, C.Muramatsu, N.Kamiya, M.Zhang, D.Fukuoka, Y.Hatanaka, T.Matsubara, A.Teramoto, Y.Uchiyama, H.Chen, and H.Hoshi: A01-3 Model Construction for Computational Anatomy: Progress Overview FY2012, Proc. of the Fourth International Symposium on the Project "Computational Anatomy", 22-42, (2013)

[6] X.Zhou, A.Watanabe, X.Zhou, T.Hara, R.Yokoyam, M.Kanematsu, and H.Fujita: Automatic organ segmentation on torso CT images by using content-based image retrieval, Proc. of SPIE Medical Imaging, Vol.8314, 83143E-1 - 83143E-7, (2012).

[7] X.Zhou, S.Wang, H.Chen, T.Hara, R.Yokoyama, M.Kanematsu, H.Hoshi and H.Fujita: Automatic localization of solid organs on 3D CT images by a collaborative majority voting decision based on ensemble learning, Computerized Medical Imaging and Graphics, Vol.36, No.4, 304-313, (2012).

[8] X.Zhou and H.Fujita: Automatic organ localization on X-ray CT images by using ensemble learning techniques, in Machine learning in computer-aided diagnosis: Medical imaging intelligence and analysis, ed. by K.Suzuki, 403-418, IGI Global, USA, (2012).

[9] X.Zhou, A.Yamaguti, X.Zhou, T.Hara, R.Yokoyam, M.Kanematsu, and H.Fujita, "Automatic organ localizations on 3D CT images by using majority-voting of multiple 2D detections based on local binary patterns and Haar-like features," Proc. of SPIE medical imaging, 8670, 86703A-1 - 86703A-7, 2013.

[10] X.Zhou, T.Ito, X.Zhou, T.Hara, R.Yokoyam, M.Kanematsu, and H.Fujita, "A universal approach for automatic organ segmentations on 3D CT images based on organ localization and 3D GrabCut" Proc. of SPIE medical imaging, in press, 2014.

[11] S.Yamaguchi, X.Zhou, R.Xu, T.Hara, R.Yokoyama, M.Kanematsu, H.Hoshi, S.Kido, and H.Fujita: Construction of statistical shape models of organs in torso CT scans using MDL method, Proc. of International Forum on Medical Imaging in Asia, P2-33, 2012.

[12] X.Zhou, R.Xu, T.Hara, Y. Hirano, R.Yokoyama, M. Kanematsu, H. Hoshi, S. Kido, and H. Fujita, "Developments and evaluation of the statistical shape modeling for principal inner organs on torso CT images", Radiological Physics and Technology, in press, (2014).

[13] M.Zhang, X.Zhou, S.Goshima, H.Chen, C.Muramatsu, T.Hara, R.Yokoyama, M.Kanematsu, and H.Fujita: An application to pulmonary emphysema classification based on model of texton learning by sparse representation, Proc. of SPIE Medical Imaging, Vol.8315, 831534-1 - 831534-7, (2012).

[14] M.Zhang, X.Zhou, H.Chen, C.Muramatsu, T.Hara, R.Yokoyama, M.Kanematsu, and H.Fujita: Pulmonary emphysema classification based on an improved texton learning model by sparse representation, Proc. of SPIE Medical Imaging, 8670, 86700F-1 - 86700F-7, (2013).

[15] N. Kamiya, X. Zhou, H. Chen, C. Muramatsu, T. Hara, R. Yokoyama, M. Kanematsu, H. Hoshi, and H. Fujita: Automated segmentation of psoas major muscle in X-ray CT images by use of a shape model: Preliminary study, Radiological Physics and Technology, vol.5, no.1, pp.5-14, 2012.

[16] N.Kamiya, X.Zhou, H.Chen, C.Muramatsu, T.Hara, and H.Fujita: Model-based approach to recognize the rectus abdomens muscle in CT images, IEICE Transactions on Information and Systems, Vol.E-96-D, No.4, 869-871, (2013).

[17] N. Kamiya, C. Muramatsu, X. Zhou, H. Chen, T. Hara, H. Hoshi and H. Fujita: Automated recognition of the lateral abdominal muscles in CT images by use of a virtual image: Unfolding technique, Proc. of 69th scientific congress of Japanese Society of Radiological Technology, 173, (2013).

[18] H. Kobayashi, N. Kamiya, A. Kamiya, X. Zhou, H. Chen, C. Muramatsu, T. Hara and H. Fujita: Model-based approach to recognize the middle and inferior fibers of the trapezius muscle in torso CT images, IEICE Technical Report, Vol.113, No. 410, 69-72, (2014), in Japanese.

[19] Y.Shimizu, T.Suzuki, T.Kobayashi, T.Hara, X.Zhou, S.Ito, S.Kumita, K.Ishihara, T.Katafuchi, and H.Fujita: Evaluation of anatomical registration method for torso FDG-PET scans, IEICE Technical Report, Vol.MI2011-78, 7-10, (2012), in Japanese.

[20] Y.Shimizu, T.Hara, D.Fukuoka, X.Zhou, C.Muramatsu, T.Kobayashi, S.Ito, S.Kumita, K.Ishihara, T.Katafuchi, and H.Fujita: Diagnosis support for cancer trteatment on torso FDG-PET/CT scans by using anatomical standization method, JAMIT, (2012), in Japanese.

[21] Y.Shimizu, T.Hara, D.Fukuoka, X.Zhou, C.Muramatsu, S.Ito, K.Hakozaki, S.Kumita, K.Ishihara, T.Katafuchi, and H.Fujita: Temporal subtraction system on torso FDG-PET scans based on statistical image analysis, Proc. of SPIE Medical Imaging, 8670, 86703F-1 - 86703F-6, (2013).

[22] Y.Shimizu, T.Hara, D.Fukuoka, X.Zhou, C.Muramatsu, S.Ito, K.Hakozaki, S.Kumita, K.Ishihara, T.Katafuchi, and H.Fujita: Analysis and construction of normal model on torso FDG-PET scans based on lean body mass, IEICE Technical Report, Vol.MI2013-74, 97-101, (2014).

[23] T.Matsumoto, T.Hayashi, T.Hara, A.Katsumata, C.Muramatsu, X.Zhou, Y.Iida, M.Matsuoka, K.Katagi, and H.Fujita: Automated scheme for measuring mandibular cortical thickness on dental panoramic radiographs for osteoporosis screening, Proc. of SPIE, Vol. 8315, 83152L16, (2012).

[24] C.Muramatsu, T.Matsumoto, T.Hatashi, T.Hara, A.Katsumata, X.Zhou, Y.Iida, M.Matsuoka, T.Wakisaka, and H.Fujita: Automated measurement of mandibular cortical width on dental panoramic radiographs, International Journal of Computer Assisted Radiology and Surgery, Vol. 8, No.6, 877-885, (2013).

[25] C.Muramatsu, T.Nakagawa, A.Sawada, Y.Hatanaka, T.Yamamoto, and H.Fujita: Automated determination of cup-do-disc ratio for classification of glaucomatous and normal eyes on stereo retinal fundus images, J Biomed Optics, Vol. 16, No.9, 096009-1-8, (2011).

[26] C.Muramatsu, T.Nakagawa, A.Sawada, Y.Hatanaka, T.Yamamoto, and H.Fujita: Automated segmentaion of optic disc region on retinal fundus photographs: Comparison of contour modeling and pixel classification methods, Comput. Methods Programs Biomed, Vol.101, 23-32, (2011).

[27] C.Muramatsu, Y.Hatanaka, K.Ishida, A.Sawada, T.Yamamoto, and H.Fujita: Preliminary study on differentiation between glaucomatous and non-glaucomatous eyes on stereo fundus images using cup gradient models, Proc. SPIE Medical Imaging, in press, (2014).

[28] Y.Uchiyama, T.Asano, H.Kato, M.Kanematsu, H.Hoshi, T.Iwama, and H. Fujita : Computer-aided diagnosis for detection of lacunar infarcts on MR images – ROC analysis of radiologists' performance-, Journal Digital Imaging, Vol.25, No.4, 497-503, (2012).

[29] Y.Uchiyama, T.Hara, J.Shiraishi, M.S.Chung, and H.Fujita: Improvement of CAD scheme for classification of lacunar infarcts and enlarged Virchow Robin spaces using Visible Korean Human Image, Proc. of International Forum on Medical Imaging in Asia, O5-2, (2012).

[30] A. Abe Y.Uchiyama, C.Muramatsu, T.Hara, J.Shiraishi, and H.Fujita: Improvement of CAD scheme for detection of lacunar infarcts on MR images by using template matching, Medical Imaging and Information Science, Vol.30, No.2, 39-43, (2013), in Japanese.

[31] A.Tanigawa, Y.Uchiyama, C.Muramatsu, T.Hara, J.Shiraishi, and H.Fujita: Improvement of CAD scheme for detection of lacunar infarcts in MR images using AdaBoost template matching, IEICE technical report, Vol.113, No.410, 323-326, (2014), in Japanese.

[32] A.Teramoto and H.Fujita: Fast lung nodule detection in chest CT images using cylindrical nodule-enhancement filter, International Journal of Computer Assisted Radiology and Surgery, Vol.8, No.2, 193-205, (2013).

[33] A.Ikeya, A.Teramoto, T.Hara, and H.Fujita: Improving nodule detection in chest CT images using a cylindrical filter based on the anatomical structure of the lung, Med. Imag. Tech., Vol.30 No.5, 293-297, (2012), in Japanese.

[34] A.Teramoto, H.Fujita, K.Takahashi, O.Yamamuro, T.Tamaki, M.Nishio, and T.Kobayashi: Hybrid method for the detection of pulmonary nodules using positron emission tomography/computed tomography: A preliminary study, International Journal of Computer Assisted Radiology and Surgery, Vol.9, No.1, 59-69, (2014).

[35] N.Yamada, T.Matsubara, A.Tsunomori, T.Hara, C.Muramatsu, T.Endo, and H.Fujita: Comparison of automated detection performance of architectural distortion on two kinds of mammograms, Proc. of International Forum on Medical Imaging in Asia 2012, Vol.64, (2012).

[36] H.Nawa, T.Watanabe, D.Fukuoka, N.Terabayashi, T.Hara and H.Fujita: Development of image analysis and quantitative evaluation of the Locomotive syndrome, IEICE Technical Report, Vol.111, No.389, MI2011-133, 311-314, (2012), in Japanese.

[37] H.Nawa, T.Watanabe, D.Fukuoka, N.Terabayashi, T.Hara, and H.Fujita: 3D image analysis of gastrocnemius muscle for quantitative evaluation of the Locomotive syndrome, IEICE Technical Report, Vol.112, No. 411, MI2012-75, 69-70, (2013), in Japanese.

[38] C.Muramatsu, K.Nishimura, M.Oiwa, M.Shiraiwa, T.Endo, K.Doi, and H.Fujita: Correspondence among subjective and objective similarities and pathologic types of breast masses on digital mammography, IWDM, Springer Lectures Notes in Computer Science (LNCS) series, Vol.7361, 450-457, (2012).

[39] C.Muramatsu, K.Nishimura, T.Endo, M.Oiwa, M.Shiraiwa, K.Doi, and H.Fujita : Representation of lesion similarity by use of multidimensional scaling for breast masses on mammograms, Journal Digital Imaging, Vol.26, No.4, 740-747, (2013).

[40] M.Zhang, X.Zhou, S.Goshima, H.Chen, C.Muramatsu, T.Hara, R.Yokoyama, M.Kanematsu, and H.Fujita: An application to pulmonary emphysema classification based on model of texton learning by sparse representation, Proc. of SPIE Medical Imaging, Vol.8315, 831534-1 - 831534-7, (2012).

[41] H.Watanabe, M.Kanematsu, T.Kitagawa, Y.Suzuki, H.Kondo, S.Goshima, K.Kajita, K.T. Bae, Y.Hirose, S.Miotani, X.Zhou, and H.Fujita: MR elastography of the liver at 3 T with cine-tagging and bending energy analysis: Preliminary results, European Radiology, Vol.20, 2381-2389, (2010).

[42] S.Goshima, M.Kanematsu, T.Kobayashi, T.Furukawa, X.Zhang, H.Fujita, H.Watanabe, H.Kondo, N.Moriyama, and K.T.Bae: Staging hepatic fibrosis: Computer-aided analysis of hepatic contours on gadolinium ethoxybenzyl diethylenetriaminepentaacetic acid-enhanced hepatocyte-phase magnetic resonance imaging, Hepatology, Vol.55, No.1, Letter, 328-329, (2012).

[43] R.Xu, X.Zhou, Y.Hirano, R.Tachibana, T.Hara, S.Kido, and H.Fujita: Particle system based adaptive sampling on spherical parameter space to improve the MDL method for construction of statistical shape models, Computational and Mathematical Methods in Medicine, vol.2013, Article ID 196259, 9 pages, (2013).

BOOKS, BOOK CHAPTERS AND REVIEWS:

[44] H.Fujita, T.Ishida, and S.Katsuragawa (eds.): Handbook of Practical Image Analysis in Medicine, Ohmsha, Tokyo, Japan, (2012), in Japanese.

[45] C.Muramatsu and H.Fujita: Detection of Eye Diseases, in Computer-aided Detection and Diagnosis in Medical Imaging, eds. by Q.Li and R.Nishikawa, Chap.19, in press, Taylor & Francis Books, Inc., (2014).

[46] Y.Uchiyama and H.Fujita: Detection of Cerebrovascular Diseases, in Computer-aided Detection and Diagnosis in Medical Imaging, eds. by Q.Li and R.Nishikawa, Chap.17, in press, Taylor & Francis Books, Inc., (2014).

[47] T.Hayashi, H.Chen, K.Miyamoto, X.Zhou, T.Hara, and H.Fujita: Computer-aided image analysis for vertebral anatomy on X-ray CT images (Chapter 7), ed. by K.Suzuki, in Computational Intelligence in Biomedical Imaging, 159-184, (2014).

[48] H.Chen, X.Zhou, H.Fujita, M.Onozuka, and K.Kubo: Age-related changes in trabecular and cortical bone microstructure, International Journal of Endocrinology, Vol.2013, Article ID 213234, 1-9, (2013).

[49] H.Jiang, Z.Ma, M.Zong, H.Fujita, and X.Zhou: Abdomen CT image segmentation based on MRF and ribs fitting approach, Chapter 10, Lecture Notes in Electrical Engineering, Vol.206, 75-81, (2013).

[50] T.Hayashi, H.Chen, K.Miyamoto, X.Zhou, T.Hara, and H.Fujita: Computer-aided image analysis for vertebral anatomy on X-ray CT images (Chapter 7), ed. by K.Suzuki, in Computational Intelligence in Biomedical Imaging, 159-184, Springer, New York, (2014).

LIST OF ACCEPTED AND PUBLISHED PAPERS SINCE 1ST APRIL 2013

[1] X.Zhou, A.Yamaguti, X.Zhou, T.Hara, R.Yokoyam, M.Kanematsu, and H.Fujita: Automatic organ localizations on 3D CT images by using majority-voting of multiple 2D detections based on local binary patterns and Haar-like features, Proc. of SPIE Medical Imaging 2013: Computer-Aided Diagnosis, 8670, 86703A-1 - 86703A-7, (2013).

[2] M.Zhang, X.Zhou, H.Chen, C.Muramatsu, T.Hara, R.Yokoyama, M.Kanematsu, and H.Fujita: Pulmonary emphysema classification based on an improved texton learning model by sparse representation, Proc. of SPIE Medical Imaging 2013: Computer-Aided Diagnosis, 8670, 86700F-1 - 86700F-7, (2013).

[3] Y.Shimizu, T. Hara, D. Fukuoka, X.Zhou, C.Muramatsu, S.Ito, K.Hakozaki, S.Kumita, K.Ishihara, T.Katafuchi, H.Fujita: Temporal subtraction system on torso FDG-PET scans based on statistical image analysis, Proc. of SPIE Medical Imaging 2013: Computer-Aided Diagnosis, 8670, 86703F-1 - 86703F-6, (2013).

[4] R.Yoshikawa, A.Teramoto, T.Matsubara, and H.Fujita: Automated detection scheme of architectural distortion in mammograms using adaptive Gabor filter, Proc. of SPIE Medical Imaging 2013: Computer-Aided Diagnosis, 8670, 86701Z-1 - 86701Z-6, (2013).

[5] S.Mori, T.Hara, M.Tagami, C.Muramatsu, T.Kaneda A.Katsumata, and H. Fujita: Automated detection of abnormalities in paranasal sinus on dental panoramic radiographs by using contralateral subtraction technique based on mandible contour, Proc. of SPIE Medical Imaging 2013: Computer-Aided Diagnosis, 8670, 86702R-1 - 86702R-6, (2013).

[6] K.Nishimura, C.Muramatsu, M.Oiwa, M.Shiraiwa, T.Endob, K.Doi, and H. Fujita: Psychophysical similarity measure based on multi-dimensional scaling for retrieval of similar images of breast masses on mammograms, Proc. of SPIE Medical Imaging 2013: Computer-Aided Diagnosis, 8670, 86701R-1 - 86701R-6, (2013).

[7] C.Muramatsu, K.Nishimura, T.Hara, and H.Fujita: Preliminary investigation on CAD system update: Effect of selection of new cases on classifier performance, Proc. of SPIE Medical Imaging 2013: Computer-Aided Diagnosis, 8670, 86701T-1 - 86701T-8, (2013).

[8] A.Abe, Y.Uchiyama, C.Muramatsu, T.Hara, J.Shiraishi, and H.Fujita: Improvement of CAD scheme for detection of lacunar infarcts on MR images by using template matching, Medical Imaging and Information Sciences, Vol.30, No.2, 39-43, (2013), in Japanese.

[9] N.Kamiya, X.Zhou, H.Chen, C.Muramatsu, T.Hara, and H.Fujita: Model-based approach to recognize the rectus abdomens muscle in CT images, IEICE Transactions on Information and Systems, Vol.E-96-D, No.4, 869-871, (2013).

[10] T.Hara, M.Tagami, S.Mori, T.Kaneda, A.Katsumata, X.Zhou, C.Muramatsu, and H.Fujita, Automated detection of paranasal sinus diseases on dental panoramic X-ray image by using contralateral subtraction technique, IEICE Transactions on Information and Systems, Vol.J96-D, No.4, 885-891, (2013), in Japanese.

[11] C. Muramatsu, T. Matsumoto, T. Hatashi, T. Hara, A. Katsumata, X. Zhou, Y. Iida, M. Matsuoka, T. Wakisaka, and H. Fujita: Automated measurement of mandibular cortical width on dental panoramic radiographs, International Journal of Computer Assisted Radiology and Surgery, Vol.8, No.6, 877-885, (2013).

[12] C.Muramatsu, R.A.Schmidt, J.Shiraishi, T.Endo, H.Fujita, and K.Doi: Usefulness of presentation of similar images in the diagnosis of breast masses on mammograms: Comparison of observer performances in Japan and the USA, Radiological Physics and Technology, Vol.6, No.1, 70-77, (2013).

[13] C.Muramatsu, K.Nishimura, T.Endo, M.Oiwa, M.Shiraiwa, K.Doi, and H.Fujita: Representation of lesion similarity by use of multidimensional scaling for breast masses on mammograms, Journal Digital Imaging, Vol.26, No.4, 740-747, (2013).

[14] C.Muramatsu, T.Endo, M.Oiwa, M.Shiraiwa, K.Doi, and H.Fujita: Effect of reference image retrieval on breast mass classification performance: ROC Analysis, Workshop on Breast Image Analysis in conjunction with MICCAI 2013, A.Martel, J.Hipwell, J.Schnabel, M.Neilsen, M.Nash, D.Kontos, and N.Karssemeijer (Eds), 50-57, (2013).

[15] C.Muramatsu, A.Mizukami, Y.Hatanaka, A.Sawada, T.Hara, T.Yamamoto, and H.Fujita: Improvement on recognition of major arteries and veins on retinal fundus images by template matching with vessel models, Medical Imaging and Information Sciences, Vol.30, No.3, 63-69, (2013), in Japanese.

[16] T.Inoue, Y.Hatanaka, S.Okumura, C.Muramatsu, and H.Fujita: Automated microaneurysm detection method based on eigenvalue analysis using Hessian matrix in retinal fundus images, Proc. of 35th Annual International Conference of the IEEE EMBS, 5873-5876, (2013).

[17] R.Xu, X.Zhou, Y.Hirano, R.Tachibana, T.Hara, S.Kido, and H.Fujita: Particle system based adaptive sampling on spherical parameter space to improve the MDL method for construction of statistical shape models,

Computational and Mathematical Methods in Medicine, Vol.2013, Article ID 196259, 9 pages, (2013).

[18] H.Jiang, H.Q.Tan, and H.Fujita: A hybrid method for pancreas extraction from CT image based on level-set methods, Computational and Mathematical Methods in Medicine, Vol.2013, Article ID:479516, 13 pages, (2013).

[19] H.Jiang, B.He, Z.Ma, M.Zong, X.Zhou, and H.Fujita: Liver segmentation based on snakes model and improved GrowCut algorithm in abdominal CT image, Computational and Mathematical Methods in Medicine. Vol. 2013, Article ID:958398, 12 pages, (2013).

[20] T.Sawagashira, T.Hayashi, T.Hara, A.Katsumata, C.Muramatsu, X.Zhou, Y.Iida, K.Katagi, and H.Fujita: An automatic detection method for carotid artery calcifications using top-hat filter on dental panoramic radiographs, IEICE Transactions on Information and Systems, Vol.E96-D, No.8, 1878-1881, (2013).

[21] H.Fujita, T.Hara, X.Zhou, C.Muramatsu, and N.Kamiya: Model constructions for computational anatomy: Fundamentals and applications, Medical Imaging Technology, Vol.31, No.5, 278-286, (2013).

[22] H.Fujita: Technological history of computer-aided diagnosis (CAD), Journal of IEEJ Trans., Vol.133, No.8, 556-559, (2013), in Japanese.

[23] A.Teramoto, H.Fujita, K.Takahashi, O.Yamamuro, T.Tamaki, M.Nishio, and T.Kobayashi: Hybrid method for the detection of pulmonary nodules using positron emission tomography/computed tomography: A preliminary study, International Journal of Computer Assisted Radiology and Surgery, Vol.9, 59-69, (2014).

[24] T.Hayashi, H.Chen, K.Miyamoto, X.Zhou, T.Hara, and H.Fujita: Computer-aided image analysis for vertebral anatomy on X-ray CT images (Chapter 7), ed. by K.Suzuki, in Computational Intelligence in Biomedical Imaging, 159-184, Springer, New York, (2014).

[25] X.Zhou, R.Xu, T.Hara, Y. Hirano, R.Yokoyama, M. Kanematsu, H. Hoshi, S. Kido, and H. Fujita: Developments and evaluation of the statistical shape modeling for principal inner organs on torso CT images, Radiological Physics and Technology, in press, (2014).